Draft version January 20, 2013
Preprint typeset using LaTeX style emulateapj v. 08/22/09

PULSAR OUTER-GAP ELECTRODYNAMICS: HARDENING OF SPECTRAL SHAPE IN THE TRAILING PEAK IN GAMMA-RAY LIGHT CURVE

Kouichi Hirotani[1]
Theoretical Institute for Advanced Research in Astrophysics (TIARA), Academia Sinica, Institute of Astronomy and Astrophysics (ASIAA), PO Box 23-141, Taipei, Taiwan

Draft version January 20, 2013

ABSTRACT

The spectral characteristics of the pulsed gamma-ray emission from outer-magnetospheric particle accelerators are investigated. Either positrons or electrons are accelerated outwards by the magnetic-field-aligned electric field to emit gamma-rays via curvature process. Since the particles move along relatively straight paths in the trailing side of a rotating magnetosphere, they attain higher Lorentz factors to emit more energetic gamma-rays than those in the leading side. It is first demonstrated that the cutoff energy of the curvature radiation evolves with the rotation phase owing to the variation of the curvature radii of the particle paths and maximizes at a slightly later phase of the trailing peak in the gamma-ray light curve.

Subject headings: gamma rays: stars — magnetic fields — methods: analytical — methods: numerical — stars: neutron

1. INTRODUCTION

The *Fermi* Large Area Telescope (LAT) provides a wealth of new data on isolated, rotation-powered pulsars, increasing the number of detected γ-ray pulsars from seven to more than sixty (e.g., Abdo et al. 2010a; Abdo et al. 2010b; Saz Parkinson et al. 2010). The Astro-rivelatore Gamma a Immagini LEggero (*AGILE*) has also reported the detection of about twenty γ-ray pulsars (e.g., Pellizzoni et al. 2009; Pilia et al. 2010). Since interpreting γ-rays is less ambiguous compared with reprocessed, non-thermal X-rays, the γ-ray pulsations observed from these objects are particularly important as a direct signature of basic non-thermal processes in pulsar magnetospheres, and should help to discriminate among different emission models. In this letter, we thus focus on the spectral evolution of the pulsed γ-rays and examine if the hardening of the trailing peak in the light curve, a general property derived from these observations, can be explained in the context of the outer-magnetospheric emission scenario.

The light curves and spectral evidence obtained by the observations mentioned above, suggest that the γ-ray pulsars have high-altitude emission zones whose fan-like beams scan over a large fraction of the celestial sphere. Therefore, recent pulsar high-energy emission models adopt higher-altitude emission geometries. There are three main scenarios in this approach: the outer-gap (OG) model (Cheng et al. 1986a, b; Romani 1996; Cheng et al. 2000; Hirotani 2006b, 2008; Takata et al. 2008; Romani & Watters 2010), the higher-altitude slot-gap model (Muslimov & Harding 2004), and the pair-starved polar-cap model (Frackowiak & Rudak 2005; Harding et al. 2005; Venter et al. 2009).

In the present letter, we focus on the OG model, in which pairs are created in the outer magnetosphere mainly by photon-photon (γ-γ) pair production. The produced pairs polarize owing to the magnetic-field-aligned electric field, $E_\parallel$. If the rotation and magnetic axes reside in the same hemisphere, a positive $E_\parallel$ is exerted to accelerate e^+'s (or e^-'s) outward (or inwards), increasing the real charge density outwards. The inward-migrating, relativistic e^-'s radiate curvature γ-rays, some of which (nearly head-on) collide with the X-rays emitted from the NS surface to materialize as pairs.

In a pulsar magnetosphere, there is a surface called the 'null surface', on which the Goldreich-Julian charge density (Goldreich & Julian 1969) $\rho_{\rm GJ} \equiv -\boldsymbol{B}\cdot\boldsymbol{\Omega}/(2\pi c)$ changes sign, where $\boldsymbol{B}$ denotes the local magnetic field, $\boldsymbol{\Omega}$ the NS angular-velocity vector, and c the speed of light. There is another characteristic surface called the 'light cylinder' beyond which the co-rotational velocity exceeds c. The distance of the light cylinder from the rotation axis is called the 'light-cylinder radius', $\varpi_{\rm LC} \equiv c/\Omega$, where $\Omega \equiv |\boldsymbol{\Omega}|$ denotes the NS rotational angular frequency. On each magnetic azimuthal angle φ_* (measured around the magnetic axis counter-clockwise), there is a magnetic field line that crosses the light cylinder tangentially; they are called the 'the last-open field lines'. An OG is essentially located between the null surface and the light cylinder in the higher colatitudes (i.e., in the closer region to the magnetic axis) than the last-open field lines.

2. CHARACTERISTIC ENERGY OF CURVATURE RADIATION

The characteristic energy of curvature emission is given by (e.g., Rybicki & Lightman 1979)

$$E_{\rm c} = \frac{3}{2}\gamma^3\frac{\hbar c}{\varrho_{\rm c}}, \tag{1}$$

where γ refers to the Lorentz factor of the electron or positron, $\hbar$ the Planck constant divided by 2π, and $\varrho_{\rm c}$ the curvature radius of particle's three-dimensional (3-D) motion. In the gap, the $e^\pm$'s achieve electrostatic force balance, $eE_\parallel = 2e^2\gamma^4/(3\varrho_{\rm c}^2)$, and saturate at the

Electronic address: hirotani@tiara.sinica.edu.tw
[1] Postal address: TIARA, Department of Physics, National Tsing Hua University, 101, Sec. 2, Kuang Fu Rd.,Hsinchu, Taiwan 300

terminal Lorentz factor,

$$\gamma = \left(\frac{3}{2}\frac{{\varrho_{\rm c}}^2}{e}E_\parallel\right)^{1/4}, \qquad (2)$$

where e designates the charge on the positron, and $E_\parallel$ the electric field component projected along the magnetic field line. Combining equations (1) and (2), we obtain

$$E_{\rm c} = \left(\frac{3}{2}\right)^{7/4}\hbar c {\varrho_{\rm c}}^{1/2}\left(\frac{E_\parallel}{e}\right)^{3/4}. \qquad (3)$$

Since $e^\pm$'s are saturated at γ, the spectral density of their curvature emission declines sharply as $(E/E_{\rm c})^{1/2}\exp(-E/E_{\rm c})$ above the cutoff energy, $E \gg E_{\rm c}$. Therefore, for the same $E_\parallel$, equation (3) shows that the curvature spectrum has a greater $E_{\rm c}$ for a greater $\varrho_{\rm c}$.

Since the pair production mainly takes place between the inward γ-rays and the surface X-rays, most of the pairs are produced in the lower altitudes where the X-ray density is large and the collisions take place mostly head-on. Thus, outward-moving species (e.g., e^+'s) run longer distances than inward ones within the gap, leading to a stronger outward γ-ray flux than the inward one. Therefore, to elucidate the physical mechanism that produces harder spectrum in the trailing peak of a γ-ray light curve, we concentrate on the outward-moving particles and the resultant outward emissions in § 2

To reveal the nature of curvature radiation, we must consider the curvature radius of actual particle motion in the 3-D pulsar magnetosphere. Well inside the light cylinder, the drift motion due to magnetic curvature, magnetic gradient, or time-varying electric field is small compared to the $\boldsymbol{E}\times\boldsymbol{B}$ drift. Thus, particles co-rotate with the magnetic field lines. In the flaring field line geometry of a NS magnetosphere, the path of outward-moving particles can be illustrated as figure 1. In the leading side, particle's path is bent towards the rotational direction as the thin solid curve indicates. However, in the trailing side, the path is straighter as indicated by the thick solid curve. Thus, outward-moving particles have greater curvature radii in the trailing side than in the leading side. This leads to a greater $E_{\rm c}$ in equation (3). This is the qualitative reason why most of the γ-ray pulsars detected with LAT exhibits harder spectrum in the trailing light-curve peak than in the leading peak.

Next, let us examine the distribution of the curvature radius more quantitatively. Due to strong relativistic beaming, curvature photons are emitted along the instantaneous particle velocity measured by the distant static observer (i.e., us). In the polar coordinates, the orthonormal components of the particle velocity become (Mestel et al. 1985; Camenzind 1986a,b)

$$\frac{v^r}{c} = f_{\rm v}\frac{B^r}{B}, \quad \frac{v^{\hat\theta}}{c} = f_{\rm v}\frac{B^{\hat\theta}}{B}, \quad \frac{v^{\hat\phi}}{c} = f_{\rm v}\frac{B^{\hat\varphi}}{B} + \frac{\varpi}{\varpi_{\rm LC}}, \quad (4)$$

where $\gamma \gg 1$ is assumed and

$$f_{\rm v} \equiv -\frac{\varpi}{\varpi_{\rm LC}}\frac{B^{\hat\varphi}}{B} \pm \sqrt{1-\left(\frac{\varpi}{\varpi_{\rm LC}}\right)^2\left(\frac{B_{\rm p}}{B}\right)^2}; \qquad (5)$$

$B_{\rm p} \equiv \sqrt{(B^r)^2+(B^{\hat\theta})^2}$, B denotes the strength of the magnetic field, ϖ the distance from the rotation axis.

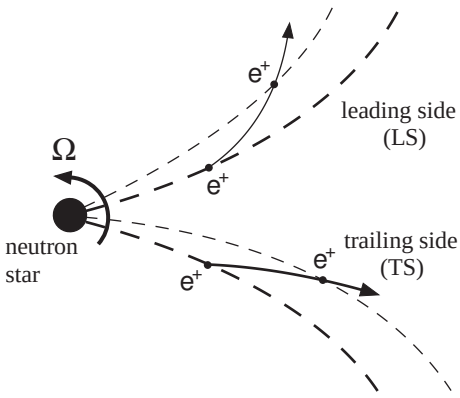

FIG. 1.— Schematic figure (top view) of particle motion in a rotating pulsar magnetosphere. The thick dashed lines represent the dipolar magnetic field lines at some moment, and the thin dashed ones do the same field lines at later rotation phase. The thin and thick solid lines represent the paths of particles moving outwards in the leading side (LS) and trailing side (TS), respectively.

Both $(v^r,v^{\hat\theta},v^{\hat\phi})$ and $(B^r,B^{\hat\theta},B^{\hat\varphi})$ are measured by a distant static observer (i.e., in the inertial observers frame). The upper sign of $f_{\rm v}$ (eq. [5]) corresponds to the outward motion along the magnetic field line, whereas the lower sign to the inward motion. These expressions are quite general and valid irrespective of the force balance on the particles as long as $\gamma \gg 1$, because they are derived only from the Maxwell equations and the frozen-in condition, the latter of which is justified since we consider $E_\parallel \ll B$ (or equivalently, consider that the potential drop in the gap is much small compared to the electro-motive force exerted on the spinning NS surface). For example, they are valid not only for $e^\pm$'s being accelerated without dissipation but also for those in the force balance between radiation-reaction and electro-static acceleration. Note that equations (4) and (5) correspond to a generalization of § 4.1 of Dyks et al. (2010) into the higher altitudes. Note also that equations (4) and (5) are applicable not only within the light cylinder but also outside of it and that $B^{\hat\varphi} < 0$ holds in ordinary situations.

Integrating equation (4) along particle motion, we obtain the path of the particle, which allows us to compute $\varrho_{\rm c}$ as a function of the distance s along the field line. Since the incorporation of a field-line deformation due to magnetospheric currents is out of the scope of this letter, we adopt a retarded, vacuum dipole field (Cheng et al. 2000) as an example. In figure 2, we present $\varrho_{\rm c}/\varpi_{\rm LC}$ as a function of s for a representative magnetic field line in the leading side (LS; $\varphi_* = +60°$) and that in the trailing side (TS; $\varphi_* = -60°$), where φ_* refers to the magnetic azimuthal angle measured around the magnetic axis counter-clockwise. The magnetic inclination angle, α, is assumed to be 60°.

In figure 2, the (red) thick solid and dashed curves denote $\varrho_{\rm c}/\varpi_{\rm LC}$ of the actual particle path, whereas the (black) thin solid and dashed curves do $\varrho_{\rm c}/\varpi_{\rm LC}$ of the last-open magnetic field lines. The LS quantities are plotted with dashed curves, while the TS quantities with solid curves. It follows that $\varrho_{\rm c}/\varpi_{\rm LC}$ of the particle path (labeled with P-TS) becomes greater than that of the field line (B-TS) in the TS. In the LS, on the contrary, $\varrho_{\rm c}/\varpi_{\rm LC}$ of the particle path (P-LS) becomes less than that of the field line (B-LS). Note that B-TS is corrected

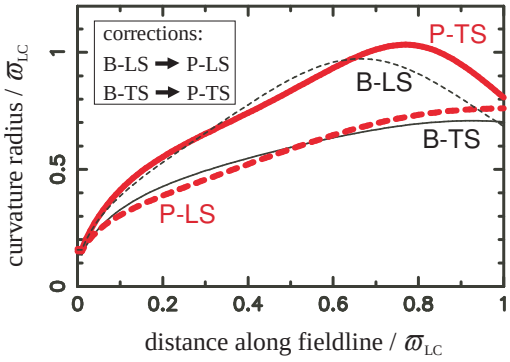

FIG. 2.— Distribution of the curvature radius, $\varrho_{\rm c}$ as a function of the distance along the magnetic field line. Both the abscissa and the ordinate are normalized by the light cylinder radius, $\varpi_{\rm LC}$. The (red) thick solid curve (labeled as P-TS) denotes $\varrho_{\rm c}/\varpi_{\rm LC}$ of the actual particle path in the TS (specifically, at $\varphi_* = -60°$). The (red) thick dashed curve (P-LS) denotes $\varrho_{\rm c}/\varpi_{\rm LC}$ of the actual particle path in the LS ($\varphi_* = 60°$). The (black) thin solid curve (B-TS) does $\varrho_{\rm c}/\varpi_{\rm LC}$ of the last-open magnetic field line in the TS ($\varphi_* = -60°$), while the (black) thin dashed curve (B-LS) that of the last-open magnetic field line in the LS ($\varphi_* = 60°$).

to P-TS and B-LS to P-LS, and that the magnetic field lines (see B-LS vs. B-TS) have greater $\varrho_{\rm c}$ in the LS whereas the particle paths (P-LS vs. P-TS) have greater $\varrho_{\rm c}$ in the TS. In previous pulsar emission models, it has been phenomenologically assumed that the particles emit curvature radiation along local magnetic field lines and adopted B-LS and B-TS as $\varrho_{\rm c}/\varpi_{\rm LC}$; thus, it has been impossible to reproduce a harder spectrum in the TS than the LS. Precisely speaking, they did considered the aberration of photon momentum to compute the emission direction from each point (and to reproduce the observed pulse profiles), but have computed $\varrho_{\rm c}$ from the magnetic field geometry (as represented by the thin lines labeled with B-LS and B-TS). Instead, we should take account of particle's' motion with equation (4) and adopt the correct $\varrho_{\rm c}$ (as represented by P-LS and P-TS); then, we obtain a harder spectrum in the TS as observed from most of the γ-ray pulsars.

3. SELF-CONSISTENT ACCELERATOR SOLUTION

To precisely compute the phase-resolved spectrum, we must solve $E_\parallel$ and the distribution functions of $e^\pm$'s at each point in the 3-D pulsar magnetosphere, together with the radiative transfer. In this section, we thus solve the set of Maxwell and Boltzmann equations in the 3-D pulsar magnetosphere in the open zone from the NS surface to the light cylinder under appropriate boundary conditions (see Hirotani 2006a, b for details). To demonstrate general spectral properties, we consider typical young NS parameters, $P = 0.1$ s, $\dot{P} = 10^{-13}$ s s^{-1}, $kT_{\rm s} = 50$ eV, where kT refers to the blackbody temperature of the whole NS thermal emission. For this 'example pulsar', we adopt $\alpha = 60°$.

We present the distribution of the gap in the magnetosphere by showing the gap fractional thickness, $h_{\rm m}$, projected on the last-open field line surface in figure 3. If $h_{\rm m} = 1.0$, it means that all the open fluxes threads the OG. On the other hand, if $h_{\rm m} \ll 1$, only the fluxes very close to the last-open field lines are active. It follows that the gap exist mainly outside the null surface (white curve); thus, the present solution coincidentally corresponds to a quantitative extension of previous, phenomenological OG models.

We next present the distribution of photon emission as a function of NS rotational phase and the observers' viewing angle ζ in figure 4, where the distance is assumed to be 1 kpc. Since only the photons emitted from the OG connected to the north magnetic pole are plotted, photons propagating into the southern hemisphere ($\zeta > 90°$) are mostly emitted by outward-moving charges, whereas photons into $\zeta < 90°$ are by inward ones. Thus, we find that the outward photon flux dominates the inward one.

We can find the pulse profiles by slicing across the photon intensity plot in figure 4 at a constant ζ. As an example, we choose $\zeta = 115°$ and show the pulse profile in figure 5 as the dashed line (in arbitrary unit); P1 corresponds to the leading peak, while P2 the trailing peak. One full NS rotation period is depicted in the abscissa.

Finally and most importantly, we examine the evolution of spectral properties with phase. To this aim, we fit the solved differential photon flux (photons cm^{-2} s^{-1} MeV^{-1}) with a power law with exponential cutoff shape given by

$$\frac{dN}{dE} = KE^{-\Gamma}\left(-\frac{E}{E_{\rm c}}\right) \qquad (6)$$

in each phase bin with 1/72 (i.e., 5°) interval, where both E and $E_{\rm c}$ are in GeV unit and refer to the photon energy and the cutoff energy, respectively; Γ is the photon index. The best fit Γ and $E_{\rm c}$ are depicted in figure 5. The (red) thick solid curve in the top panel denotes the evolution of Γ with phase, while that in the bottom panel that of $E_{\rm c}$. For comparison, Γ and $E_{\rm c}$ that would be obtained if we adopted $\rho_{\rm c}$ of the magnetic field lines (instead of that of the particle path) are also depicted by thin dotted curves. It follows that the photon index remains roughly constant during the bright phase, while the cutoff energy sharply peaks in the trailing peak as expected from the analytic argument in § 2. Note that only comparable $E_{\rm c}$ would be obtained in the two light-curve peaks if we adopted $\rho_{\rm c}$ of the magnetic field lines (as in previous pulsar emission models). The conclusion of greater $E_{\rm c}$ in the trailing peak is, in deed, consistent with the spectral properties of most of the γ-ray pulsars detected with LAT (for PSR J2021+3651, see Abdo et al. 2009; for the Crab pulsar, see Abdo et al. 2010b; for the Vela pulsar, see Abdo et al. 2010c; for PSR J1057–5226, PSR J1709–4429, PSR J1952+3252, see Abdo et al. 2010d; for the Geminga pulsar, see Abdo et al. 2010e).

4. DISCUSSION

By examining the actual paths of outward-moving charged particles in a 3-D pulsar magnetosphere, we demonstrated that the curvature radii of their paths become larger in the trailing side (TS) than in the leading side (LS) in § 2. Applying this result to the curvature radiation formula (§ 1), we first gave a physical explanation why the trailing peak generally exhibits a harder spectrum than the leading peak in γ-ray light curves. To confirm this analytical prediction, we solved the set of Maxwell and Boltzmann equations in the 3-D pulsar magnetosphere in § 3, finding that the obtained emissivity distribution does result in a greater cutoff energy in the trailing peak than in the leading peak. Although the discussion in § 3 is limited to the OG model, the

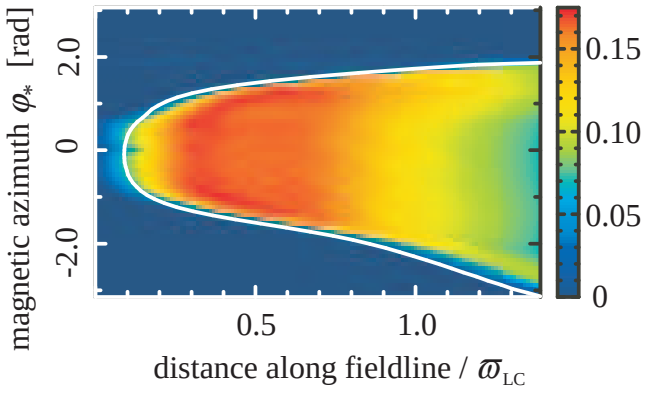

FIG. 3.— Distribution of the gap meridional thickness projected on the last-open field line surface. The white curve denotes the cross section between the last-open field lines and the null surface. The ordinate denotes the angle, φ_* [rad], measured around the magnetic axis counter-clockwise. The region $\varphi_* > 0$ (or $\varphi_* < 0$) is referred to as the leading (or trailing) side.

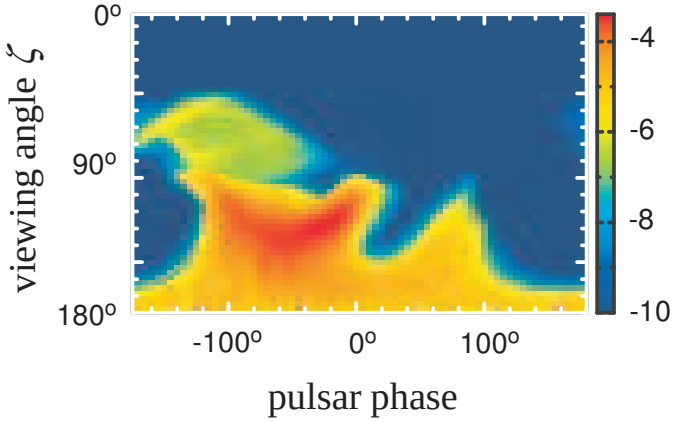

FIG. 4.— Angular distribution of photon emission above 89 MeV ($\log_{10}$ of flux per phase in MeV s^{-1} cm^{-2} deg^{-1} unit) from the outer gap connected to the north magnetic pole. The phase 0° (in the abscissa) corresponds to the neutron-star rotation phase at which the photon emitted from the north polar cap arrives the observer. The ordinate denotes the observer's viewing angle ζ with respect to the rotation axis.

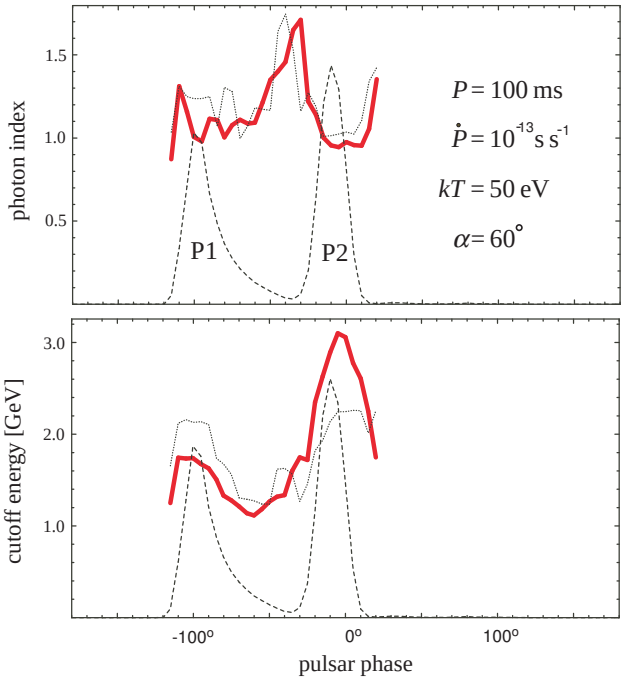

FIG. 5.— Evolution of the photon index Γ (top panel) and the cutoff energy $E_{\rm c}$ (bottom panel) with the rotational phase, is depicted by the (red) thick solid curve, for an example pulsar with $P = 0.1$ s, $\dot{P} = 10^{-13}$ s s^{-1}, $kT = 50$ eV, and $\alpha = 60°$. Observer's viewing angle is assumed to be $\zeta = 115°$. For comparison, Γ and $E_{\rm c}$ that would be obtained if we adopted the curvature radii of the magnetic field lines (instead of the particle paths) are depicted by the thin dotted curves. Pulse profile is overlaid as the dashed curves (in arbitrary unit).

same argument can be, in fact, readily applied to other higher-altitude emission models, as long as the emission is due to the curvature process. What we have to change is to amend $E_\parallel$ (instead of what is obtained in the OG model) as a function of position in the 3-D pulsar magnetosphere. Unless $E_\parallel$ becomes substantially greater in the LS than in the TS, the same conclusion will be derived, which is, in deed, expected both in the slot-gap and in the pair-starved polar-cap models.

In figure 5, Γ peaks at pulsar phase $\sim -30°$. However, this peaking structure of Γ appears at small-flux phase, and hence is vulnerable to the choice of ζ. For example, it disappears for $\zeta > 120°$. On the contrary, the peaking structure of $E_{\rm c}$ at a slightly later phase of the trailing peak, is generally obtained in a wide parameter range of $(P,\dot{P},kT,\alpha)$ and ζ. Although not all the parameter space has not been investigated, the conclusion that the trailing peak has a greater cutoff energy than in other phases, appears to be universal.

In this letter, we have adopted a retarded, vacuum dipole magnetic field. However, in general, we should take account of the deformation of the field lines due to the magnetospheric current (Contopoulos et al. 1999; Gruzinov 2005; Spitkovsky 2006; Bai & Spitkovsky 2010a, b; Contopoulos & Kalapotharakos 2010). The effect of deformation works to straighten the field lines in the outer magnetospheres, pushing the OG position towards the light cylinder particularly in the TS; for example, if $\alpha = 60°$, the OG within the region $\varphi_* < -60°$ is suggested to be less active due to the position shift towards the light cylinder. Nevertheless, the self-consistent OG solution presented in § 3 shows that the pair production is not, any way, self-sustained in $\varphi_* < -60°$, resulting in a negligible emission from this region. For example, the trailing peak (around $-10°$ in pulsar phase) is mostly formed by the emission from $-60° < \varphi_* < -30°$. In addition, the specific intensity towards $\zeta \sim 115°$ direction will not be strongly affected by the straightening, which follows from panel (d) of figure 8 in Bai and Spitkovsky (2010b). On these grounds, we consider that the conclusions in the present letter are relatively less vulnerable to the correction of the field-line geometry due to magnetospheric currents.

We can further apply the present numerical method to any rotation-powered pulsars. In subsequent papers, we will demonstrate that the numerical solutions are consistent with various observations of individual pulsars, such as the energy fluxes, pulse profiles, and phase-resolved spectra. To this aim, it is essential to self-consistently solve the screening processes due to the polarization of the produced pairs, together with the distribution functions of $e^\pm$'s and photons. This can be achieved only by

solving the Maxwell and Boltzmann equations simultaneously in the 3-D pulsar magnetosphere.

This work is supported by the Theoretical Institute for Advanced Research in Astrophysics (TIARA) operated under Academia Sinica, the National Science Council Excellence Projects program in Taiwan administered through grant number NSC 96-2752-M-007-006-PAE, and the Formosa Program between National Science Council in Taiwan and Consejo Superior de Investigaciones Cientificas in Spain administered through grant number NSC100-2923-M-007-001-MY3.

REFERENCES

Abdo, A. A. et al. 2009, ApJ, 700, 1059
Abdo, A. A. et al. 2010a, ApJS, 187, 460
Abdo, A. A. et al. 2010b, ApJ, 708, 1254
Abdo, A. A. et al. 2010c, ApJ, 713, 146
Abdo, A. A. et al. 2010d, ApJ, 720, 26
Abdo, A. A. et al. 2010e, ApJ, 720, 272
Bai, X. N., & Spitkovsky, A. 2010a, ApJ, 715, 1270
Bai, X. N., & Spitkovsky, A. 2010b, ApJ, 715, 1282
Camenzind, M. A & A, 156, 137
Camenzind, M. A & A, 162, 32
Cheng, K. S., et al. 1986a ApJ, 300, 500
Cheng, K. S., et al. 1986b ApJ, 300, 522
Cheng, K. S. et al. 2000, ApJ, 537, 964
Contopoulos, I., Kazanas, D., and Fendt, C. 1999, ApJ, 511, 351
Contopoulos, I. & Kalapotharakos, C. 2010 MNRAS, 404, 767
Dyks, J. et al. 2010, MNRAS, 509, 405
Frackowiak, M., Rudak, B. 2005, Adv. Space Res., 35, 1152
Goldreich, P. Julian, W. H. 1969, ApJ, 157, 869
Gruzinov, A. 2005, Phys. Rev. Letters 94, 021101
Harding, A. K. et al. 2005, ApJ, 622, 531
Hirotani, K. 2006, ApJ, 652, 1475 (H06a)
Hirotani, K. 2006, Mod. Phys. Lett. A (Brief Review) 21, 1319–1337 (H06b)
Hirotani, K. 2008, ApJ, 688, L25
Mestel, L. et al. 1985, MNRAS, 217, 443
Muslimov, A. G., & Harding, A. K., 2004, ApJ, 617, 471
Pellizzoni, A. et al. 2009, ApJ, 695, L115
Pilia, M. et al. 2010, ApJ, 723, 707
Romani, R. W. 1996, ApJ, 470, 469
Romani, R. W., & Watters, K. 2010, ApJ714, 810
Saz Parkinson, P. M. et al. ApJ, 725, 571
Spitkovsky, A. 2006, ApJ, 648, L51
Takata, J.et al. 2008, MNRAS, 386, 748
Venter, C. et al. 2009, ApJ, 707, 800